Domain wall motion damped by the emission of spin waves

R. Wieser, E. Y. Vedmedenko, and R. Wiesendanger
Institut für Angewandte Physik und Zentrum für Mikrostrukturforschung, Universität Hamburg, Jungiusstrasse 11, D-20355 Hamburg, Germany
(Received 16 October 2009; published 11 January 2010)

The domain wall motion of field-driven transverse domain walls in biaxial ferromagnets is investigated by solving the Landau-Lifshitz-Gilbert equation. It is demonstrated that with increasing easy-plane or hard-axis anisotropy D_h different types of domain wall motion occur. The different scenarios correspond to different velocity equations. In the limit of absent hard-axis anisotropy ($D_h/J=0$) a precessional domain wall motion can be found while for $D_h/J\neq 0$ a steady domain wall motion interrupted by a Walker breakdown at high fields prevails. In the limit of huge anisotropies ($D_h/J\gg 0$) a domain wall motion damped by emission of spin waves occurs. The connection between magnetic systems and the theory of solitons is discussed.

DOI: 10.1103/PhysRevB.81.024405 PACS number(s): 75.10.Hk, 75.40.Mg, 75.60.Ch

I. INTRODUCTION

Domain wall motion in magnetic nanowires has been extensively studied during the last years. The idea behind is to construct logic[1] and data-storage devices[2,3] based on domain wall motion. The physical picture of domain wall motion has been strongly influenced by the publications of Walker.[4,5] He demonstrated that above a critical field the domain wall starts to oscillate and, therefore, the velocity decreases with increasing field. Below this so-called Walker breakdown field one finds a steady domain wall motion with the velocity increasing with increasing field. The experimental proof of the existence of the Walker threshold[6,7] ensured the popularity of this theory. Recently, however, it has been demonstrated that the reality is much more complicated and the domain wall motion also depends on the shape and material of the wire. For instance, while the transverse domain walls in thin-film structures show the behavior described by Walker[8–11] one finds a totally different domain wall motion in cylindrical nanowires.[12–14] In this case the transverse domain wall shows a precessional motion and the Walker breakdown does not occur.

Further, it has been shown that vortex domain walls do not show a Walker breakdown as well.[15] Instead of a Walker breakdown the vortex domain wall starts to emit spin waves and its velocity decreases. A similar phenomenon is well known in the theory of Solitons,[16–19] where this behavior is known as "Bremsstrahlung."[20] Many analytical descriptions of this phenomenon based on a perturbation theory can be found in literature[21–25] but so far, there is neither a numerical proof nor a clear understanding of the reason for the spin-wave emission. The dispersion relationship are unknown as well. In the following we clarify the above-mentioned questions by performing numerical simulations. Further, we give a quantitative description of spin-wave emission of the transverse domain wall by calculating the dispersion of the emitted spin waves.

The paper is organized as follows. After introduction (Sec. I) and model description (Sec. II) an overview of the theory of the transverse domain wall motion is given in Sec. III. Section IV is devoted to the investigation of spin-wave damping in transverse domain wall systems. Section V describes the connection to the theory of solitons, followed by a summary (Sec. VI).

II. MODEL

We consider a classical Heisenberg model, which might be interpreted as rigid sphere approximation of an itinerant magnet.[26,27] The magnetic properties are described by the following biaxial Hamiltonian:

$$\mathcal{H}=-J\sum_n \mathbf{S}_n\cdot\mathbf{S}_{n+1}-\mu_s\mathbf{B}\cdot\sum_n \mathbf{S}_n+D_h\sum_n (S_n^x)^2-D_e\sum_n (S_n^z)^2, \tag{1}$$

where the $\mathbf{S}_n=\mu_n/\mu_s$ are three-dimensional magnetic moments of unit length on a simple cubic lattice with the lattice constant a.

The first term in Eq. (1) describes the exchange coupling between nearest neighbors with ferromagnetic coupling constant $J>0$. The second sum is the so-called Zeeman term, which describes the coupling of the spins to an external magnetic field $\mathbf{B}$. The third sum describes an easy zy-plane or hard x-axis anisotropy ($D_h>0$). The fourth sum gives an easy-axis anisotropy ($D_e>0$) in z direction which breaks the easy-plane symmetry.

In the following we investigate a transverse domain wall in linear magnetic chains oriented along the z direction. Such chains can be interpreted as quasi-one-dimensional magnets[28–30] or as a cylindrical nanowire with a transverse domain wall.[12–15] In the second case each spin has to be interpreted as the magnetization of one layer in the xy plane $M_\alpha=\frac{1}{N}\Sigma_{n=1}^N S_n^\alpha$, $\alpha\in\{x,y,z\}$, where N is the number of spins in the layer. In such a system and in the case of the transverse domain wall the dipolar coupling plays an important role but leads to an increase in the easy-axis anisotropy $D_e=D_u+D_d$ only. Here D_u is the uniaxial anisotropy coming from the spin-orbit coupling and the second term $D_d\approx 3\zeta(3)\mu_0\mu_s^2/(4\pi a^3)$ describes the shape anisotropy coming from the dipolar interaction[15] with $\zeta(3)\approx 1.202$.

The underlying equation of motion is the Landau-Lifshitz-Gilbert (LLG) equation,

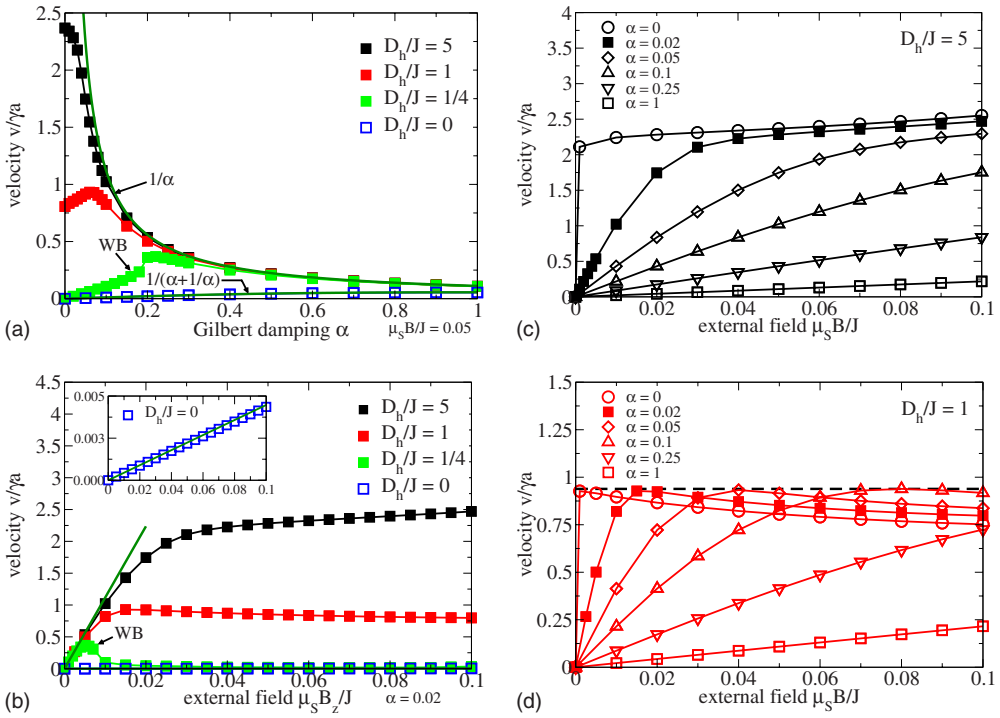

FIG. 1. (Color online) Velocity of a transverse domain wall with biaxial anisotropy (D_e and D_h) vs Gilbert damping α (a), respectively, external field $\mu_s B/J$ [(b)–(d)]. WB marks the Walker breakdown and the solid lines in (a) and (b) give the highest possible velocity given by Eq. (6). $D_e/J=0.1$, $\mu_s B/J=0.05$ [only (a)], and $\alpha=0.02$ [only (b)] are assumed.

$$\dot{\mathbf{S}}_n = -\frac{\gamma}{(1+\alpha^2)\mu_s}\mathbf{S}_n \times \mathbf{H}_n + \frac{\alpha\gamma}{(1+\alpha^2)\mu_s}\mathbf{S}_n \times (\mathbf{S}_n \times \mathbf{H}_n) \tag{2}$$

with the gyromagnetic ratio γ, the dimensionless Gilbert damping α, and the internal field given by the gradient $\mathbf{H}_n = -\partial\mathcal{H}/\partial\mathbf{S}_n$. The first term of the LLG equation describes the precessional motion of $\mathbf{S}_n$ and the second term the relaxation.

III. TRANSVERSE DOMAIN WALL MOTION

The simulations start with a relaxed head to head transverse domain wall, where the spins in the domains are oriented in $\pm z$ direction and inside the domain wall in y direction. After switching on the external field the velocity of the domain wall can be calculated either by measuring the wall displacement (zero crossing of the z component of the magnetization) or from the time dependence of the magnetization as $v = \frac{1}{2}d(\Sigma_n S_n^z)/dt$. Both methods lead to the same results.

Depending on the anisotropy one finds different cases of the magnetization reversal in combination with different velocities. Figure 1 shows the velocity as a function of the Gilbert damping α [Fig. 1(a)] and external field $\mu_s B/J$ [Fig. 1(b)] for different hard-axis anisotropies D_h/J and a constant easy-axis anisotropy $D_e/J=0.01$.

According to the literature the assumption of a zero hard-axis anisotropy $D_h/J=0$ leads to the precessional domain wall motion during magnetization reversal.[12–15] We find this behavior in our simulations as well [see Fig. 1(a)]. The corresponding velocity equation

$$v_S = \frac{\gamma B}{\alpha + 1/\alpha}\sqrt{\frac{Ja^2}{2D_e}} \tag{3}$$

for a constant domain wall width $\Delta = \sqrt{Ja^2/(2D_e)}$ and $1/(\alpha + 1/\alpha)$ velocity dependence has been derived by Slonczewski[31] and confirmed numerically.[15] In the limit of zero damping ($\alpha=0$) the velocity is zero and the magnetic moments inside the domain wall just precess around the z axis. This behavior becomes obvious when one bears in mind that for $\alpha=0$ the relaxation term in the LLG equation becomes zero.

If the hard-axis anisotropy is finite the regime which was first described by Walker[4,5] is reached [see Fig. 1(b)]. Here one finds a direct spin-flip reversal of the magnetization during the domain wall motion which corresponds to a $1/\alpha$ behavior of the velocity,

$$v_W = \frac{\gamma B}{\alpha}\sqrt{\frac{Ja^2}{2(D_e + D_h \sin^2\phi)}}. \tag{4}$$

The angle ϕ describes the angle between the plane where the spin motion takes place and the easy plane given by the hard-axis anisotropy D_h. ϕ is constant in time but depends on the external field B, the hard-axis anisotropy D_h, and the Gilbert damping α,

$$\phi = \frac{1}{2}\arcsin\left(\frac{\mu_s B}{\alpha D_h}\right). \tag{5}$$

In the limit of infinite hard-axis anisotropy $D_h/J \to \infty$ the angle ϕ becomes zero which corresponds to a magnetization

reversal strictly in the easy-axis (xy) plane. In this limit the Eq. (4) becomes

$$v_{\mathrm{LL}} = \frac{\gamma B}{\alpha}\sqrt{\frac{Ja^2}{2D_e}}. \tag{6}$$

This equation has been derived by Landau and Lifshitz in 1935 (Ref. 32) and gives the highest possible velocity of the domain wall.

Apart from the highest velocity, Eq. (5) also defines the condition for a validity of the Walker formula. For a constant Gilbert damping α a maximum value B_{max} exists (or vice versa a minimum value of the Gilbert damping α_{min} exists for a constant external field B) beyond which the Eq. (5) is no longer fulfilled. This means that the spin motion is no longer restricted to a plane and an irregular precessional motion appears. This irregular precession in combination with an asymmetric oscillating force leads to a periodic change in the domain wall width and position[4,11] which corresponds to the Walker breakdown and leads to a decrease in the velocity as one could see in Figs. 1(a) and 1(b) for $D_h/J=0.25$. In the limit of zero damping ($\alpha=0$) one finds a periodic force and back motion of the domain wall with no effective wall displacement, which means that the time-averaged velocity $\langle v\rangle$ vanishes.

A further increase in the hard-axis anisotropy leads to the elimination of the Walker breakdown. Here one finds a finite velocity of the domain wall already for $\alpha=0$ [see the $D_h/J=1$ and $D_h/J=5$ curves in Fig. 1(a)]. This is still true for an infinite hard-axis anisotropy. Here the velocity is well described by the formula of Walker [Eq. (4)] up to a maximum field value [Fig. 1(b)] or down to a minimum Gilbert damping α [Fig. 1(a)]. Beyond these limiting values the domain wall starts to emit spin waves. One can recognize that by comparing the curves for $D_h/J=1$ and $D_h/J=5$ with their $D_h/J=0.25$ counterpart in Figs. 1(a) and 1(b). In contrast to $v(\alpha)$ for $D_h/J=0.25$ the $v(\alpha)$ dependencies for stronger anisotropies ($D_h/J=1$ and $D_h/J=5$) significantly deviate from the $1/\alpha$ behavior but the velocity does not vanish for vanishing α [see Fig. 1(a)]. Additionally, the domain wall velocity for a fixed α value does not show an abrupt decrease for high fields anymore [see Fig. 1(b)].

Figures 1(c) and 1(d) give a more detailed analysis of the velocity as function of the external field for $D_h/J=5$ and $D_h/J=1$, respectively. Here several α values are inspected. As expected an increase in the Gilbert damping leads to a suppression of the spin wave.[31] This corresponds to a linear increase in the velocity with increasing magnetic field. With decreasing damping the velocity increases and one can distinguish between two regions. The (nearly) linear increase in the velocity with increasing field corresponds to a domain wall motion without spin waves while the velocity saturation corresponds to a motion with a spin-wave wake. Further, the comparison between Figs. 1(c) and 1(d) shows that although the Walker breakdown has been eliminated the velocity still decreases after a maximum velocity [marked by the dashed line in Fig. 1(d)] has been reached. This behavior shows that there is a continuous crossover from Walker breakdown to a spin-wave damped motion, where the velocity also decreases after reaching its maximum value. With decreasing hard-axis anisotropy D_h the maximum velocity as well as the corresponding field value B_{max} decrease. In the case of Fig. 1(c) the turning point appears at high fields outside the plot.

With this information at hand it is possible to understand the behavior in the region of low Gilbert damping α. The $D_h/J=1$ curve in Fig. 1(a) has been calculated with a field value $\mu_s B/J=0.05$ which leads to the decreasing velocity with decreasing damping. The same dependence calculated with a driving field of $\mu_s B/J=0.005$ would lead to the same behavior as in the case of $D_h/J=5$, which means that the domain wall emits less spin waves and moves with a higher velocity.

IV. DOMAIN WALL DECELERATION BY SPIN WAVES

To understand the physics of domain wall deceleration by spin waves described in the last section one has to answer the following two questions: what is the driving mechanism and is it possible to give a quantitative description of the spin-wave emission? To answer these questions we repeat all calculations of Sec. III in the zero damping limit ($\alpha=0$) in order to neglect the effect of all damping mechanism which are included in the Gilbert damping term.[33,34] When the driving field is switched on the domain wall starts to move. During the period between starting time t_0 and a certain time t_e the domain wall relaxes. In this starting phase the angle ϕ [see Eq. (5)] changes and the velocity of the domain wall increases. While the relaxation the Zeeman energy is absorbed by the domain wall, after t_e no additional energy could be stored inside the domain wall and the domain wall starts to emit spin waves.

With this information the driving mechanism of the spin-wave emission becomes clear. The spin-wave emission is the same as the wake behind a motorboat. This means that the spin wave is excited by the magnetization reversal of the spins inside the domain wall. The energy comes from the external field. The unexpected result of our calculations is that the domain wall moves at a constant magnetic field despite the fact that the relaxation term in the LLG equation [Eq. (2)] is skipped if $\alpha=0$. This effect can be understood taking into account the shape of the precessional motion of magnetic moments. For circular precession no domain wall motion could occur. This is the case for $D_h/J=0$. In the general case however, the hard-axis anisotropy distorts the shape of the orbit and makes it elliptic. The longer axis of the ellipse spans between the two minima of the easy-axis anisotropy. That is why the switching between these two minima becomes possible. The exchange interaction ensures an energy transfer to the neighboring spins,[35] i.e., makes the emission of spin waves behind the domain wall possible. The magnetic moments remain reversed.

For a quantitative description of the spin-wave spectra the distance dependence of the spin wave at a fixed moment of time [Fig. 2(a)] and the time dependence at a fixed lattice point [Fig. 2(b)] have to be analyzed. For that purpose the Fourier transformation in space [see inset of Fig. 2(a)] and time [see inset of Fig. 2(b)] has to be performed.[36,37] In both cases distinct peaks in the Fourier spectra have been found.

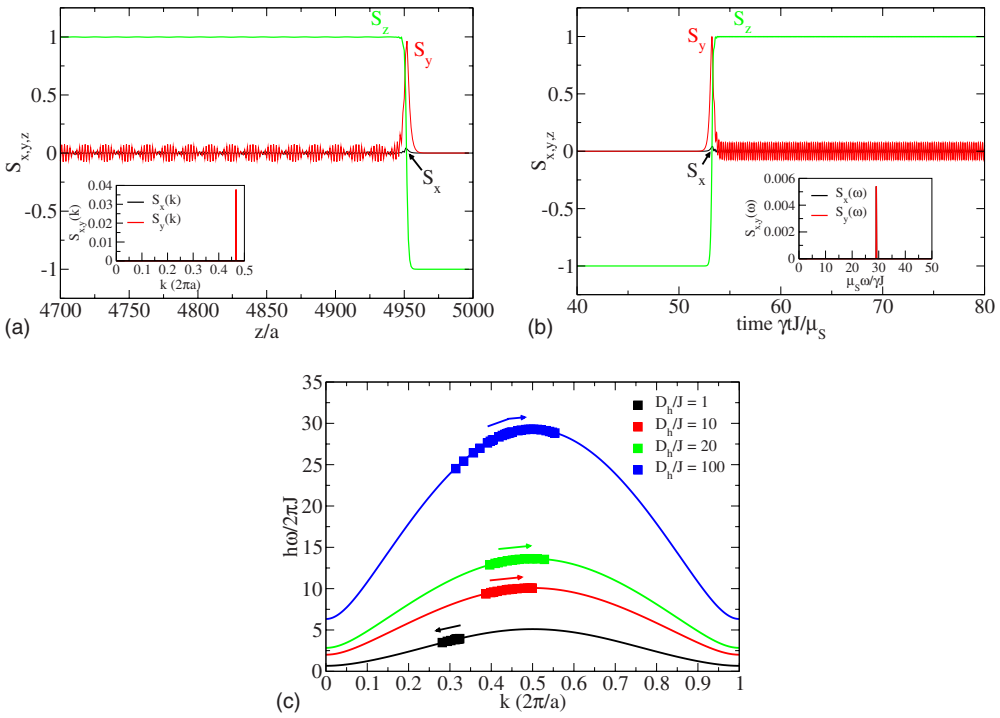

FIG. 2. (Color online) Spin wave behind a moving transverse domain wall: (a) magnetization as function of space (fixed time) and (b) magnetization as function of time (fixed space). The insets show the corresponding Fourier transformations in k, respectively, ω space. (c) Magnetic spin-wave dispersion. Solid lines are the analytical solutions given by Eq. (7). The arrows mark the direction of change (increasing/decreasing) in the wave number k with increasing applied field $\mu_s B/J$. $D_e/J=0.01$, $D_h/J=100$ [only (a) and (b)], $\alpha=0$, and $\mu_s B/J=0.005$ [only (a) and (b)], $\mu_s B/J$ between 1×10^{-6} and 1 [only (c)] are assumed.

Using these peaks the spin-wave dispersion can be plotted. The symbols in Fig. 2(c) are the numerical data for different hard-axis anisotropies D_h and field values between $\mu_s B/J = 1\times10^{-6}$ and $\mu_s B/J=1$. Each point corresponds to a single field value. The solid lines are the corresponding analytical curves given by the formula (the derivation is presented in the Appendix),

$$\frac{\hbar\omega}{J} = 2\mathcal{S}\sqrt{\left(1-\cos(ka)+\frac{D_e}{J}\right)\left(1-\cos(ka)+\frac{D_e}{J}+\frac{D_h}{J}\right)}. \tag{7}$$

Next, we would like to compare these analytical expressions with the numerical data. The Eq. (7) has been derived under the assumption of zero external field **B**. In our simulations, however, one needs to apply a finite field in order to get domain wall motion. Therefore, each symbol in Fig. 2(c) corresponds to a certain field value $\mu_s B/J$.

The interesting point of the numerical solution is that the k value has a nontrivial dependence on B. It increases with increasing field for higher values of D_h [the three upper curves in Fig. 2(c)] while decreases for weaker D_h [bottom curve in Fig. 2(c)]. This is a direct consequence of the increasing/decreasing velocity with increasing field described above [see Figs. 1(c) and 1(d)]. In other words the wave number k corresponds to the energy gained during the magnetization reversal which increases (decreases) with increasing (decreasing) domain wall velocity.[31]

With this information the physics becomes quite simple. After reaching the equilibrium the domain wall starts to emit spin waves of a certain wave number k and frequency ω. Because $\alpha=0$ has been chosen the whole energy of the system is given by the sum of the domain wall energy and the energy of the spin waves. In equilibrium the energy of the domain wall reaches some constant value depending on the in-plane angle ϕ, the applied field B, and the anisotropy D_h. The magnetization reversal, or in other words the moving domain wall, excites spin waves of a given constant energy consisting of a kinetic $\hbar\omega$ and a potential-energy contribution coming from the Zeeman term. The potential part is defined via the canting angle θ formed between the magnetic moment and the z axis while the kinetic energy is mostly determined by D_h and B.

Both energy contributions strongly depend on the reversal mechanism. In most cases the reversal is quite complicated and a mixture between the precessional motion and the direct reversal occurs. That is why the velocities found in our simulations lie somewhere between the highest possible velocity given by the formula of Landau and Lifshitz [Eq. (6)] and the lower limit given by the formula of Slonczewski [Eq. (3)]. This also means that it is impossible or quite difficult to give an analytical prediction for the velocity or the functional dependence between field values $\mu_s B/J$ and the wave number k or the potential energy.

V. CONNECTION TO SOLITONS

Whereas spin-wave emission behind a moving domain wall is an effect almost unknown in the magnetism commu-

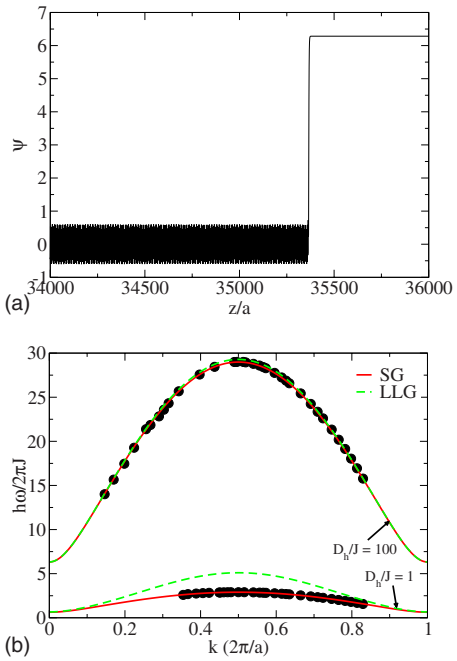

FIG. 3. (Color online) Waves behind a magnetic kink ψ as function of (a) space and (b) spin-wave dispersion. SG describes the solitonic dispersion given by Eq. (10) and LLG the magnetic dispersion [Eq. (7)]. The assumed values are $D_e/J=0.01$, $D_h/J=100$ [only (a)], $\Gamma=0$, and $f=0.005$ [only (a)], $f=7.5\times10^{-7},\ldots,0.4$ (b).

nity a similar phenomenon is well known in theory of solitons.

Following Mikeska[16,21,28,38] one can map the LLG equation [Eq. (2)] to the Sine-Gordon (SG) equation. The necessary restriction is the existence of the easy-plane geometry. The procedure leads, then, to a damped double Sine-Gordon equation,

$$\frac{\partial^2\psi}{\partial t^2} - c_0^2\frac{\partial^2\psi}{\partial z^2} + \omega_0^2 \sin\psi + f\sin\frac{\psi}{2} + \Gamma\frac{\partial\psi}{\partial t} = 0. \tag{8}$$

Here $\psi=2\theta$ with θ describing the profile of the domain wall, $\cos(\theta)=\pm\tanh(z/\Delta)$, where Δ is the domain wall width; $c_0=\sqrt{\frac{2JD_h\gamma^2}{a\mu_s}}$; $\omega_0=\sqrt{\frac{4D_eD_h\gamma^2}{a^3\mu_s}}$; $f=\frac{2\gamma^2D_hB}{\mu_s}$ is the driving field, and $\Gamma=\frac{\gamma D_h\alpha}{\mu_s}$ is the damping constant.

Using Eq. (8), we have performed the same simulation as before for the case of the magnetic domain walls. Starting with the relaxed static Kink solution ($f=0$, $\Gamma=0$) of Eq. (8),

$$\psi = 4\arctan[\exp(\pm z/\Delta)]. \tag{9}$$

The driving field $f\neq0$ accelerates the Kink. After reaching the equilibrium the Soliton starts to emit spin waves. Then, the spin-wave dispersion for $\Gamma=0$ can be calculated in the same manner as before, with aid of Fourier transformations in space and time. Figure 3(b) shows the comparison between the magnetic spin-wave dispersions (LLG) given by Eq. (7) and the Sine-Gordon spin-wave dispersions (SG) given by[16]

$$\omega^2 = 2c_0^2[1-\cos(ka)]/a^2 + \omega_0^2. \tag{10}$$

As one can see there is an excellent agreement between the numerical data (points) and the analytical curves (solid lines) given by Eq. (10). The dashed lines represent the analytical dispersion curves given by Eq. (7). It can be seen that for small D_h the magnetic spin-wave (LLG) and SG solutions differ while with increasing hard-axis anisotropy D_h the dispersion curves of the magnetic and soliton system become identical. This can be understood on the basis of the fact that with increasing anisotropy D_h the reversal becomes more direct ($\dot{\phi}\to0$) and the magnetization reversal takes place in the easy plane given by D_h. In this case the angle ϕ [see Eq. (5)] becomes zero. This assumption, however, just leads to the double Sine-Gordon equation. For $D_h/J=100$ this assumption is nearly fulfilled and both dispersion curves (magnetic and solitonic) coincide. This is not the case for $D_h/J=1$. Here the assumption is not fulfilled and a strong deviation occurs. Hence, applications of the double Sine-Gordon equation is reasonable only for $D_h/J\gg1$.

VI. SUMMARY

We have investigated the domain wall motion of the field-driven transverse domain walls in biaxial ferromagnets. We show that with increasing easy-plane or hard-axis anisotropy D_h different types of domain wall motion occur. In the limit of absent hard-axis anisotropy ($D_h/J=0$) the transverse domain wall shows a precessional motion. Here, the velocity is well described by the equation given by Slonczewski. For finite hard-axis anisotropy ($D_h/J\neq0$) the transverse domain wall shows a steady-state motion. For small anisotropies ($D_h>0$) this velocity is limited by the occurrence of a Walker breakdown. For higher D_h the Walker breakdown is eliminated and a spin-wave damped domain wall motion emerges. We have analyzed the emitted spin waves and calculated the spin-wave dispersion numerically and analytically. In the limit of huge hard-axis anisotropies D_h the LLG equation [Eq. (2)] has been mapped to a damped double Sine-Gordon equation [Eq. (8)]. The connection of spin waves behind a moving transverse domain wall and behind a magnetic kink is discussed. Further, we have calculated the solitonic spin-wave dispersion analytically as well as numerically.

ACKNOWLEDGMENTS

This work has been supported by the Deutsche Forschungsgemeinschaft in the framework of subproject B3 of the SFB 668 and by the Cluster of Excellence "Nanospintronics."

APPENDIX: DERIVATION OF EQ. (7)

To obtain the dispersion Eq. (7) one has to solve the LLG Eq. (2). In the case of vanishing damping α, nearest-neighbor interaction and without external field $\mu_s\mathbf{B}$ the LLG equation is given by

$$\frac{d\mathbf{S}_n}{dt} = \frac{\gamma}{\mu_s}[J\mathbf{S}_n \times (\mathbf{S}_{n-1} + \mathbf{S}_{n+1}) + 2D_e(\mathbf{S}_n \times S_n^z \hat{\mathbf{z}}) - 2D_h(\mathbf{S}_n \times S_n^x \hat{\mathbf{x}})]. \quad \text{(A1)}$$

Under the assumption of a small amplitude of excitation: $S_z \approx +S$; $S_x, S_y \ll S$, Eq. ((A1) becomes

$$\frac{dS_n^x}{dt} \approx \frac{\gamma}{\mu_s}[-JS(S_{n-1}^y - 2S_n^y + S_{n+1}^y) + 2D_e S S_n^y],$$

$$\frac{dS_n^y}{dt} \approx \frac{\gamma}{\mu_s}[JS(S_{n-1}^x - 2S_n^x + S_{n+1}^x) - 2(D_e + D_h) S S_n^x],$$

$$\frac{dS_n^z}{dt} \approx 0.$$

These equations can be solved with the solution ansatz,

$$S_n^x = u\cos(nka - \omega t), \quad \text{(A2a)}$$

$$S_n^y = v\sin(nka - \omega t). \quad \text{(A2b)}$$

Hence, Eq. ((A1) leads to set of two coupled equations for u and v,

$$\omega u = \frac{2S\gamma}{\mu_s}\xi v, \quad \text{(A3a)}$$

$$\omega v = \frac{2S\gamma}{\mu_s}[\xi + D_h]u \quad \text{(A3b)}$$

with $\xi = \{J[1 - \cos(ka)] + D_e\}$.

Equations ((A3) have a solution if

$$\begin{vmatrix} \omega & -\frac{2S\gamma}{\mu_s}\xi \\ -\frac{2S\gamma}{\mu_s}[\xi + D_h] & \omega \end{vmatrix} = 0$$

thus, with $\gamma = \frac{g\mu_B}{\hbar}$ and $\mathcal{S} = \frac{g\mu_B}{\mu_s}S$ lead to the spin-wave dispersion Eq. (7),

$$\hbar\omega = 2\mathcal{S}\sqrt{\xi[\xi + D_h]}. \quad \text{(A4)}$$

Substituting ω in Eq. (A3) leads to the ellipticity,

$$\frac{v}{u} = \frac{\hbar\omega}{2\mathcal{S}\xi}. \quad \text{(A5)}$$

[1] D. A. Allwood, G. Xiong, C. C. Faulkner, D. Atkinson, D. Petit, and R. P. Cowburn, Science **309**, 1688 (2005).
[2] M. Hayashi, L. Thomas, R. Moriya, C. Rettner, and S. S. P. Parkin, Science **320**, 209 (2008).
[3] S. S. P. Parkin, M. Hayashi, and L. Thomas, Science **320**, 190 (2008).
[4] N. L. Schryer and L. R. Walker, J. Appl. Phys. **45**, 5406 (1974).
[5] J. F. Dillon, in *Magnetism*, edited by G. T. Rado and H. Suhl (Academic, New York, 1963), Vol. 1, p. 149.
[6] T. Ono, H. Miyajima, K. Shigeto, K. Mibu, N. Hosoito, and T. Shinjo, Science **284**, 468 (1999).
[7] S. Glathe, R. Mattheis, and D. V. Berkov, Appl. Phys. Lett. **93**, 072508 (2008).
[8] A. Thiaville and Y. Nakatani, in *Spin Dynamics in Confined Magnetic Structures III*, edited by B. Hillebrands and A. Thiaville (Springer, Berlin, 2006).
[9] M. Kläui, J. Phys.: Condens. Matter **20**, 313001 (2008).
[10] V. V. Volkov and V. A. Bokov, Phys. Solid State **50**, 1677 (2008).
[11] D. G. Porter and M. J. Donahue, J. Appl. Phys. **95**, 6729 (2004).
[12] R. Wieser, U. Nowak, and K. D. Usadel, Phase Transitions **78**, 115 (2005).
[13] H. Forster, T. Schrefl, D. Suess, W. Scholz, V. Tsiantos, R. Dittrich, and J. Fidler, J. Appl. Phys. **91**, 6914 (2002).
[14] R. Hertel and J. Kirschner, Physica B **343**, 206 (2004).
[15] R. Wieser, U. Nowak, and K. D. Usadel, Phys. Rev. B **69**, 064401 (2004).
[16] R. Wieser, E. Y. Vedmedenko, and R. Wiesendanger, Phys. Rev. B **79**, 144412 (2009).
[17] J. Yan, Y. Tang, G. Zhou, and Z. Chen, Phys. Rev. E **58**, 1064 (1998).
[18] R. L. Herman, J. Phys. A **23**, 2327 (1990).
[19] D. W. McLaughlin and A. C. Scott, Phys. Rev. A **18**, 1652 (1978).
[20] G. Eilenberger, Z. Physik B **27**, 199 (1977).
[21] H. How, R. C. O'Handley, and F. R. Morgenthaler, Phys. Rev. B **40**, 4808 (1989).
[22] H. B. Braun, Phys. Rev. B **50**, 16485 (1994).
[23] A. A. Thiele, Phys. Rev. Lett. **30**, 230 (1973).
[24] D. Bouzidi and H. Suhl, Phys. Rev. Lett. **65**, 2587 (1990).
[25] J. M. Winter, Phys. Rev. **124**, 452 (1961).
[26] V. P. Antropov, M. I. Katsnelson, B. N. Harmon, M. van Schilfgaarde, and D. Kusnezov, Phys. Rev. B **54**, 1019 (1996).
[27] B. Skubic, J. Hellsvik, L. Nordström, and O. Eriksson, J. Phys.: Condens. Matter **20**, 315203 (2008).
[28] H. J. Mikeska, J. Appl. Phys. **52**, 1950 (1981).
[29] J. K. Kjems and M. Steiner, Phys. Rev. Lett. **41**, 1137 (1978).
[30] J. P. Boucher, L. P. Regnault, J. Rossat-Mignod, J. P. Renard, J. Bouillot, and W. G. Stirling, Solid State Commun. **33**, 171 (1980).
[31] A. P. Malozemoff and J. C. Slonczewski, *Magnetic Domain Walls in Bubble Materials* (Academic, New York, 1979).
[32] D. L. Landau and E. Lifshitz, Phys. Z. Sowjetunion **8**, 153 (1935).
[33] H. Suhl, IEEE Trans. Magn. **34**, 1834 (1998).
[34] T. L. Gilbert, IEEE Trans. Magn. **40**, 3443 (2004).
[35] V. L. Safonov and H. N. Bertram, Phys. Rev. B **63**, 094419 (2001).
[36] R. W. Chantrell, J. D. Hannay, M. Wongsam, T. Schrefl, and H.-J. Richter, IEEE Trans. Magn. **34**, 1839 (1998).
[37] O. Chubykalo, J. D. Hannay, M. Wongsam, R. W. Chantrell, and J. M. Gonzalez, Phys. Rev. B **65**, 184428 (2002).
[38] H. J. Mikeska, J. Phys. C **11**, L29 (1978).